

## THE USE OF HIGH-MAGNIFICATION MICROLENSING EVENTS IN DISCOVERING EXTRASOLAR PLANETS

KIM GRIEST AND NEDA SAFIZADEH

Physics Department, University of California, San Diego, CA 92093

Received 1997 October 30; accepted 1998 January 16

### ABSTRACT

Hundreds of gravitational microlensing events have now been detected toward the Galactic bulge, with many more to come. The detection of fine structure in these events has been theorized as an excellent way to discover extrasolar planetary systems along the line of sight to the Galactic center. We show that by focusing on high-magnification events, the probability of detecting planets of Jupiter mass or greater in the lensing zone  $[(0.6-1.6)R_E]$  is nearly 100%, with the probability remaining high down to Saturn masses and substantial even at 10 Earth masses. This high probability allows a nearly definitive statement to be made about the existence of lensing-zone planets in each such system that undergoes high magnification. One might expect light-curve deviations caused by the source passing near the small primary-lens caustic to be small because of the large distance of the perturbing planet, but this effect is overcome by the high magnification. High-magnification events are relatively rare (e.g.,  $\sim 1/20$  of events have peak magnifications greater than 20), but they occur regularly, and the peak can be predicted in advance, allowing extrasolar planet detection with a relatively small use of resources over a relatively small amount of time.

*Subject headings:* gravitational lensing — planetary systems

### 1. INTRODUCTION

Microlensing has become a useful tool in astronomy for discovering and characterizing populations of objects too faint to be seen by conventional methods. By repeatedly monitoring millions of stars, several groups have now detected the rare brightenings that occur when a dark object passes between the Earth and a distant source star (Alcock et al. 1993; Aubourg et al. 1993; Udalski et al. 1993; Alard et al. 1995). These detections have now become routine, with hundreds of events reported toward the Galactic bulge, mostly by the MACHO collaboration (Alcock et al. 1996, 1997a). The reliable detection of large numbers of such lensing events allows one to use them for several auxiliary purposes. For example, relatively rare microlensing “fine-structure” events, where deviations from the simple brightening formula (Paczynski 1986; Griest 1991) are apparent, can be searched for. These have allowed several new effects to be observed, such as parallax motion (Gould 1992, 1994b; Alcock et al. 1995), the finite size and proper motion of the source star (Alcock et al. 1997b), and binary lensing (Mao & Paczynski 1991; Udalski et al. 1994; Pratt et al. 1995).

Here we consider the special case of binary lensing when one (or more) of the companions is actually a planet orbiting the primary lens. This possibility has been investigated by several groups, starting with Mao & Paczynski (1991) and Gould & Loeb (1992). They found the remarkable result that detectable fine structure occurs relatively frequently even for rather low-mass planets. For example, Gould & Loeb (1992) find for a Jupiter-mass planet 5 AU from a solar-mass star that the probability of detecting the fine structure caused by the Jupiter-mass planet is about 17%, while for a Saturn-like planet the probability is about 3%. These relatively high probabilities occur when the planet is in the “lensing zone,” which will be discussed later, but they imply that many planetary systems could be discovered if a systematic search for microlensing fine structure were made. The light-curve deviations caused by a

planet last only a few hours or days (depending on the mass of the planet) and can occur at any time during the much longer ( $\sim 40$  days) primary lensing event. In order not to miss these short excursions, round-the-clock monitoring would be required, implying dedicated telescopes at several locations. In return, dozens to hundreds of planetary detections could be made, more than by any other proposed detection method. Thus, microlensing may be the best way to gather statistics on the frequency, mass distribution, and semimajor axis distribution of planets. Microlensing is also sensitive to planetary systems throughout the Galaxy and not just in the solar neighborhood, as are most other planet search techniques. The main disadvantage to microlensing is that further study of individual systems is probably impossible.

Following the early work, contributions have been made by several other groups. Bolatto & Falco (1994) calculated detection probabilities; Bennett & Rhie (1996) and Wambsgans (1997) extended to Earth-mass planets by including the finite source effect; Gaudi & Gould (1997) discussed extraction of physical parameters from observational data; and Tytler (1996), Peale (1997), and Sackett (1997) calculated the number of expected detections for realistic observing strategies.

### 2. MICROLENSING FORMULAS, CAUSTICS, AND MAGNIFICATION MAPS

Microlensing occurs when an intervening stellar-mass lens passes close to the line of sight between an observer and a distant source star. For Galactic distances, if the lens is a single-point mass, two images form with a separation of milliarcseconds, which is too small to resolve. However, since the sum of the areas of the images is larger than the projected area of the source, the magnification, which is given by the ratio of these areas, can be significant. When the source lies directly behind the lens, the image becomes a ring of radius  $R_E$ , and the magnification theoretically becomes infinite. Points in the source plane where the mag-

nification is infinite are called caustics, and the positions of the images of these caustics are called critical curves. For a single lens, the caustic is single point behind the lens, and the critical curve is the Einstein ring.

The scale of the microlensing effect is set by the Einstein ring:

$$R_E = \left[ \frac{4Gm_l Lx'(1-x')}{c^2} \right]^{1/2} = 612 R_\odot \times \left[ \frac{m_l}{M_\odot} \frac{L}{\text{kpc}} x'(1-x') \right]^{1/2}, \quad (1)$$

where  $m_l$  is the mass of the primary lens,  $L = D_{\text{os}}$  is the distance to the source star,  $x' = D_{\text{ol}}/D_{\text{os}}$  is the fractional distance of the lens,  $R_\odot$  is the solar radius, and  $M_\odot$  is the solar mass. Throughout, we will scale all lengths to  $R_E$ . For convenience, note that 1 AU is  $214.94 R_\odot$ .

When the lens consists of two pointlike objects, the caustic positions and shapes depend on the planet-to-lens mass ratio  $q = m_p/m_l$  and the projected planet-lens separation  $x_p$ . The primary lens is assumed to reside at the origin, and the planet is along the positive  $x$ -axis at  $x_p$  in units of  $R_E$ . For arbitrary distances and mass ratios, the caustic structure can be complicated, but for small values of  $q$ , and for an  $x_p$  that is not precisely unity, the picture is simple. The pointlike single-lens caustic becomes a tiny wedgelike caustic, still located near  $x = 0$ , while one or two new caustics appear depending on the planet position. For planets far from the lens ( $x_p > 1$ ), there is one new caustic, a small diamond-shaped planetary caustic located on the same side of the lens as the planet, while for  $x_p < 1$ , two small heart-shaped caustics appear close together on the opposite side of the lens. As discussed in the Appendix, the position of these caustics is given approximately by  $x_c \approx (x_p^2 - 1)/x_p$ . Figure 1 shows the caustics for the case of  $q = 0.003$ , corresponding to a Jupiter-mass planet around a  $0.3 M_\odot$  star.

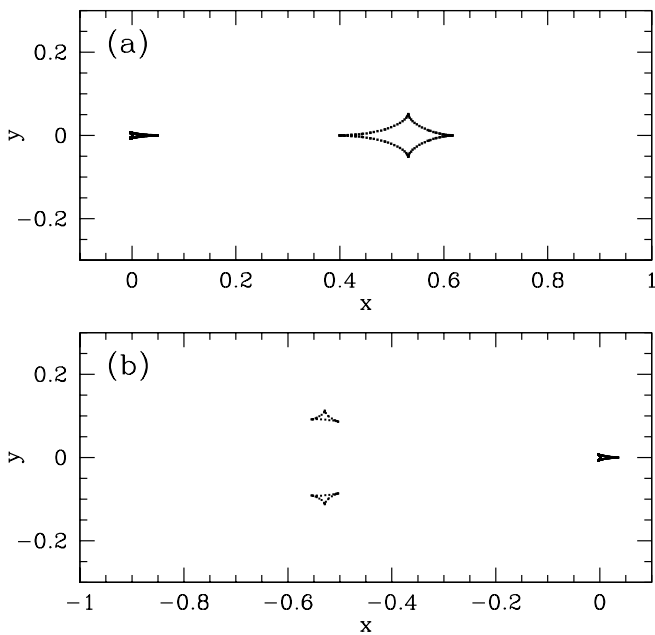


FIG. 1.—Caustics for  $q = 0.003$ , showing the central primary caustic near the origin and the larger planetary caustics. Panel (a) is for a planet at  $x_p = 1.3$ , and panel (b) is for the “dual” position at  $x_p = 1/1.3 = 0.769$ .

Panel (a) is for  $x_p = 1.3$ , and panel (b) is for  $x_p = 1/1.3 = 0.769$ . We will call the caustic near  $x = 0$  the “central” or “primary-lens” caustic and the other caustics the “planetary” caustics.

The relative motion of the source, lens system, and observer can be described as the source moving behind a static lens plane described by the projected positions of the lens, planet, and caustics. We work in the lens plane throughout and project physical sizes such as the source stellar radius into dimensionless numbers in the lens plane by multiplying by  $x'$  and dividing by  $R_E$ . If the planet orbits the primary lens in a plane other than the lens plane, its position is also projected into the lens plane.

For single-point lenses, high-magnification events occur when the source comes near the caustic at  $x = 0$ . If  $u$  is the projected distance of the source from the lens (in units of  $R_E$  in the lens plane), the magnification is  $A = (u^2 + 2)u^{-1}(u^2 + 4)^{-1/2} \sim u^{-1}$  for large  $A$ . The peak magnification  $A_{\text{max}}$  occurs at  $u_{\text{min}}$ , the distance of closest approach. The trajectory intersects a circle of radius  $u_{\text{min}}$  at its closest approach, with  $\beta$  being the angle between this intersection point and the positive  $x$ -axis. With the addition of a planet, we continue to define high-magnification events as those caused by the source approaching the central caustic. For planetary-mass binary systems, the light curve will be very close to that of a single lens for most of its duration.

Planetary fine structure in the high-magnification case will arise because of the difference between a point caustic and the wedgelike central caustic. If  $A \sim 1/u$  as the source approaches the caustic, then the size of the deviation  $\delta = dA/A \sim -A du$ , where  $du$  is the shift in the caustic position due to the planet. It is shown in the Appendix that the size of the central caustic along the  $x$ -axis is

$$u_c \approx \frac{qx_p}{(x_p - 1)^2} \quad (2)$$

and that this formula is invariant under a “duality” transformation  $x_p \rightarrow 1/x_p$ . As described in the Appendix, this formula is good for  $q \ll 1$  and  $x_p$  not near unity. Thus, for high-magnification events, we expect deviations of order

$$\delta \sim u_c A. \quad (3)$$

This estimate of light-curve deviation is in rough agreement with the more precise calculations of the next sections, and the caustic size estimate (eq. [2]) is excellent, as can be seen in Figure 2. Figure 2 shows close-ups of the central caustic for various planetary positions and planetary-mass ratios. The  $x_p \rightarrow 1/x_p$  symmetry is also apparent in these figures. Magnification maps of the source plane projected onto the lens plane are especially useful when discussing the detection of planets or the probability of certain types of events occurring. These are formed by imagining a source at each point in the plane and calculating the resulting image sizes and resulting magnifications. Observationally, one measures the microlensing light curve, the apparent brightness of a star, as a function of time, and this is completely described by a track through this magnification map. The duration of the event depends on the size of the Einstein ring and the relative projected transverse speed  $v_\perp$  of the lens system. We will divide all times by  $t_E = R_E/v_\perp$ , so the time to cross the Einstein ring diameter is  $\Delta t = 2.0$ .

Examples of magnification maps and the resulting light curves can be found in Wambsganss (1997), Gould & Loeb

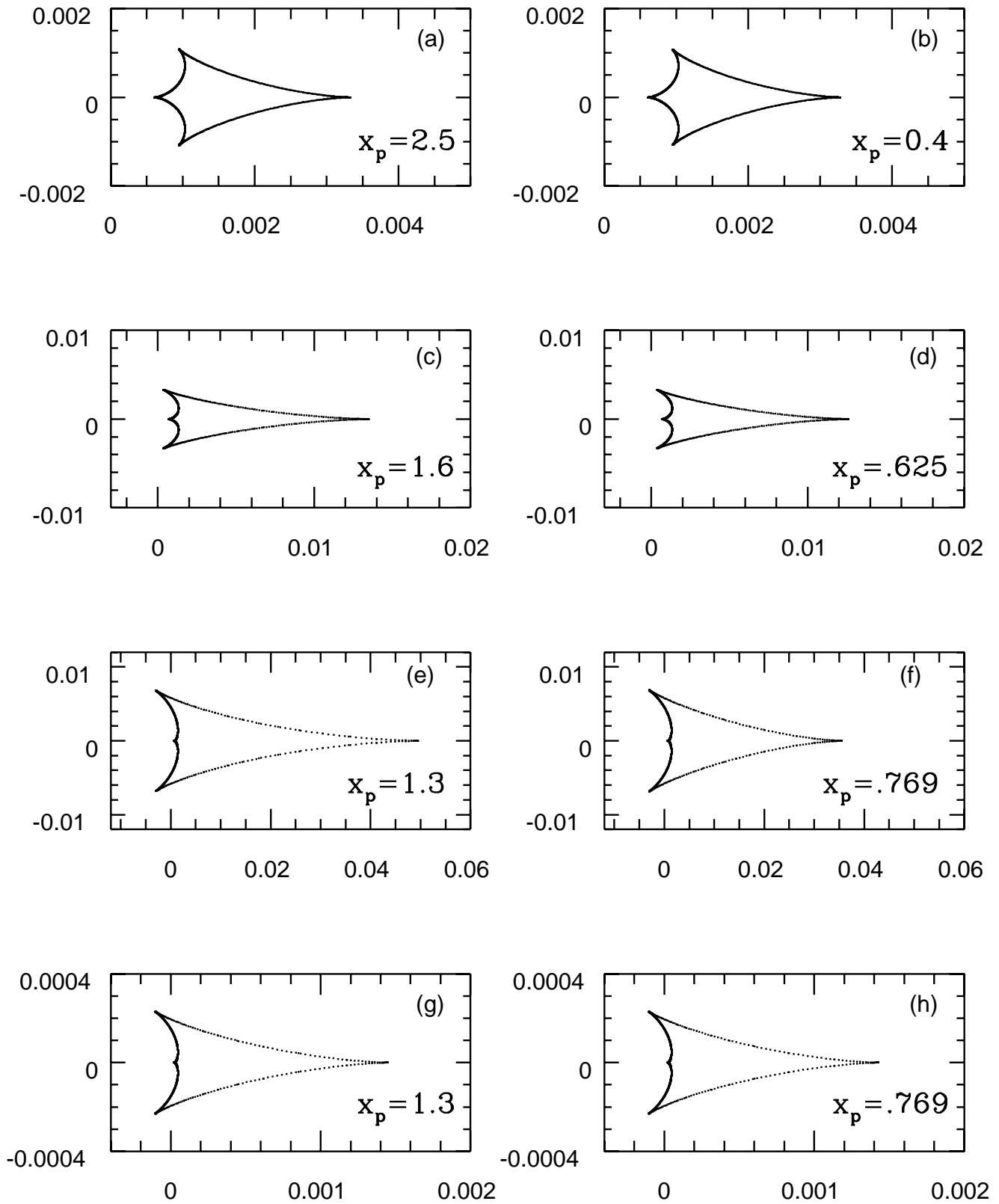


FIG. 2.—Close-ups of the central primary lens caustic. Left-hand panels show planetary positions  $x_p > 1$ , while right-hand panels show a planet in the dual positions  $1/x_p$ . All panels except (g) and (h) have  $q = 0.003$ . Note the excellent match of left-hand and right-hand panels, except for (e) and (f), where the approximation is just starting to break down. Panels (g) and (h) are for  $q = 0.0001$ , where the caustics are predicted to be 30 times smaller and symmetry is restored.

(1992), and several other places. Figure 3 shows some example maps, and Figure 4 shows some example light curves.

There are several techniques to calculate such maps in practice. For pointlike lenses, the lens equation in complex notation is given by (e.g., Witt 1990)

$$z_s = z + \sum_j m_j / (\bar{z}_j - \bar{z}), \quad (4)$$

where  $z_j = x_j + iy_j$  are the positions of the point masses in the lens plane,  $z_s = x_s + iy_s$  is the position of the source,  $z = x_i + iy_i$  is the position of the images, and the overbar denotes complex conjugation. We can rescale this equation by dividing all lengths by  $R_E$  and all masses by  $m_i$  and specialize to just one planet to get

$$z_s = z - 1/\bar{z} + q/(x_p - \bar{z}). \quad (5)$$

One sees that the mapping from an image position at  $z$  to a source position at  $z_s$  is one to one and extremely simple; however, the reverse mapping requires solving the above equation for  $z$  and results in a fifth-degree polynomial in  $z_s$  (see, e.g., Witt 1990). The partial magnifications are given by the Jacobian of the mapping from the source to lens plane evaluated at the image positions:

$$A_i = \left( 1 - \frac{\partial z_s}{\partial \bar{z}} \frac{\partial \bar{z}_s}{\partial \bar{z}} \right)^{-1}, \quad (6)$$

where the sign of  $A$  gives the parity of the image, and in our case  $\partial z_s / \partial \bar{z} = 1/\bar{z}^2 + q/(\bar{z} - x_p)^2$ . Caustics and critical curves are found as points where  $A_i = \infty$ . The total magnification is just the sum of the absolute values,  $A = \sum_i |A_i|$ .

The most direct way to create a magnification map is to solve for  $A$  at each point in the source plane by solving the fifth-degree polynomial. When the source is inside a caustic there are five images, while if the source is outside the caustics there are two spurious solutions and only three images. In the latter case, one of these images is behind the lens and is very small, and the other two are important. A complication of this approach occurs when the mass of the planet is small. The magnification map varies on scales smaller than the planetary Einstein ring  $R_p$ , which can be small compared with the size of the projected source star radius. Thus, one must integrate the magnification over the limb-darkened source profile to get an accurate total magnification. The caustic structure gives rise to singularities in  $A$ , which make this integration tricky. (See Bennett & Rhie 1996; Gould & Gaucherel 1997; and Gaudi & Gould 1997 for examples of this approach.) We have developed computer programs that successfully implement this approach, but they are rather slow.

Alternatively, one can note the simplicity of the mapping from image to source plane and simply cover the image plane densely with “photons” and then map them back to their source positions. The resulting density of source photons is proportional to the ratio of image to source areas and therefore proportional to the magnification. See Wambsganss (1997) for an example of this method. This method intrinsically incorporates the finite source effect since one must bin the source photons. The bin size is the effective source size. To consider a larger source size or to include a round source with limb darkening, one merely convolves the magnification map with a kernel made from the desired source profile. We mainly used this method in

creating our maps, although we checked them in various ways using direct solution.

Light curves of single-lens microlensing are simple smooth curves (Paczynski 1986; Griest 1991), while if a planet exists there can, in addition, be several sharp peaks. The durations of these peaks typically scale with  $R_p \propto q^{1/2}$  and last only a day or two, or even only a few hours, compared with the typical primary lens event duration of 40 days (Alcock et al. 1997a). A nice set of examples of both magnification maps and light curves can be found in Wambsganss (1997). For both maps and light curves we plot residuals:

$$\delta = \frac{\Delta A}{A} = \frac{A_{\text{binary}} - A_{\text{single}}}{A_{\text{single}}}. \quad (7)$$

In Figure 3 we show some maps for  $q = 10^{-4}$ . Figure 3a shows  $x_p = 1.3$ , where there is only one planetary caustic, and Figure 3b shows  $x_p = 0.8$ , where there are two planetary caustics on the other side of the central caustic. The light curves in Figure 4 are for  $q = 0.003$ ,  $x_p = 1.5$ ,  $u_{\min} = 0.05$ , and various angles of approach. Note the relatively simple structure of these high-magnification light curves (with the exception of the trajectory along the  $x$ -axis, which also hits the planetary caustic).

The method of magnification maps lets us investigate the effects of sources of different radii. Once a high-resolution map is produced, it can be quickly convolved with any of various source sizes and profiles, and the light curves and probabilities can be recomputed. For our convolution kernel we use a limb-darkened profile given by  $I(r) = 0.4 + 0.6(1 + r^2/R_*^2)^{1/2}$ , where  $R_*$  is the stellar radius,  $r$  is the distance from the center of the star, and  $I$  is normalized to give a total flux equal to the preconvolution flux. The maps in Figures 3a and 3b were convolved with a kernel of radius  $u_* = 0.003$ , while Figure 3c is for a source radius of  $u_* = 0.03$ . Note that these radii are in units of the Einstein ring (eq. [1]) and projected into the lens plane. So, for example, a typical main-sequence bulge star of radius  $R_* = 3 R_\odot$  projects to  $u_* = 0.003$  if the lens is at 4 kpc and to  $u_* = 0.0084$  if the lens is at 7 kpc. The source is assumed to be at 8 kpc and the primary lens to have  $m_l = 0.3 M_\odot$  in these examples. A giant star of radius  $10 R_\odot$  projects to  $u_* = 0.01$  for  $x' = 0.5$ , and  $u_* = 0.028$  for  $x' = 0.875$ . The map of Figure 3c is therefore descriptive of a  $30 R_\odot$  star with a lens system at 4 kpc or a  $10 R_\odot$  source with a lens system at 7 kpc. An interesting feature of Figure 3c is the circular ring around the central caustic. There is a jump in magnification as the limb of the source star crosses the caustic. However, as the star covers more of the region around the caustic, a cancellation occurs since there is a negative deviation on one side of the caustic and a positive deviation on the other.

In Figure 5 we show the result of increasing source size on the deviation light curves. The light curves are all for  $q = 10^{-4}$ ,  $x_p = 1.3$ ,  $u_{\min} = 0.02$ , and  $\beta = 50^\circ$ . As expected (Gould 1994a; Nemiroff & Wickramasinghe 1991; Witt & Mao 1994; Alcock et al. 1997b), as the source radius increases the amplitude of the signal decreases and the duration of the deviation increases. When the star radius is increased to  $u_* = 0.03$ , then it actually crosses the central caustic, giving rise to two bumps on the light curve. These bumps occur when the trajectory crosses the ring seen in Figure 3c. If detected, these bumps are very useful since the star is in effect resolved and the time between the bumps

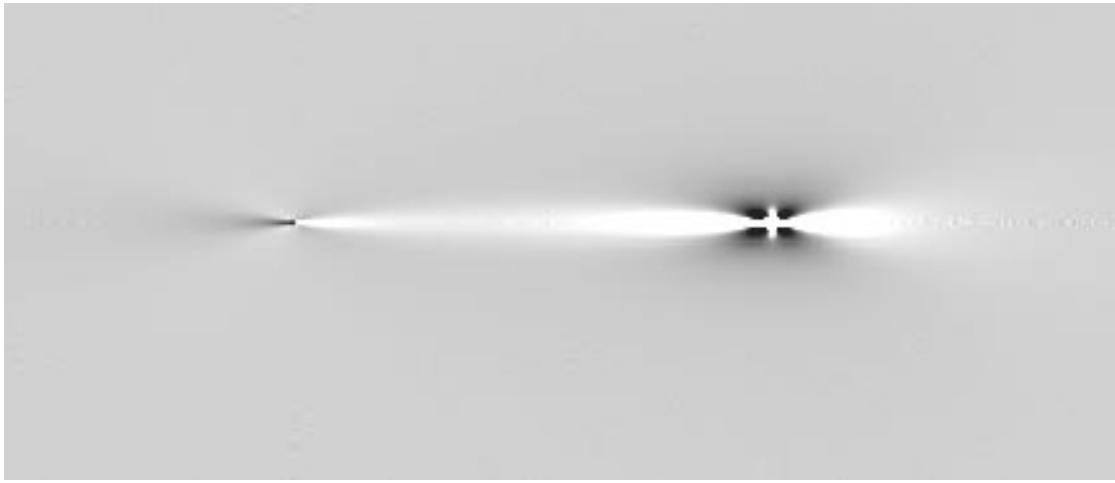


FIG. 3a

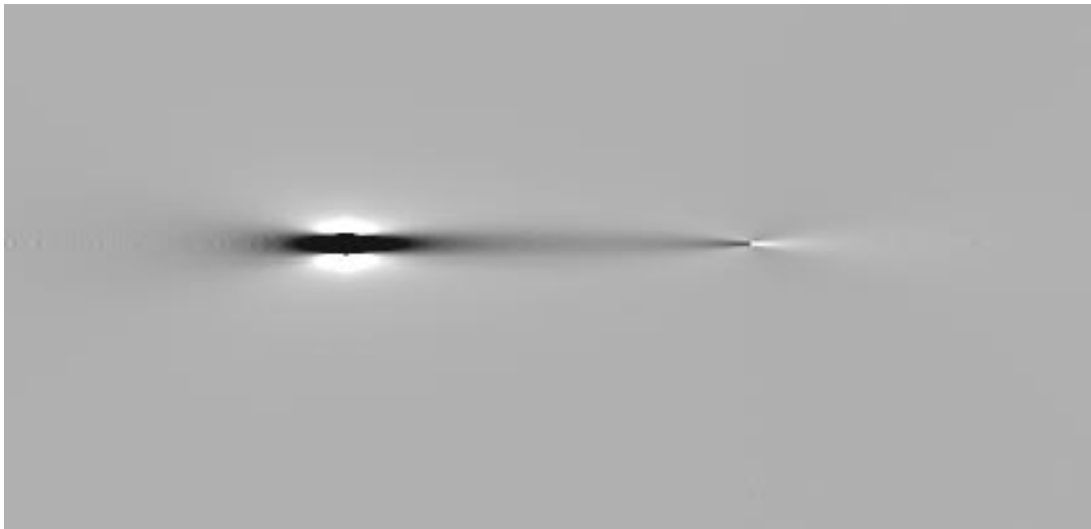


FIG. 3b

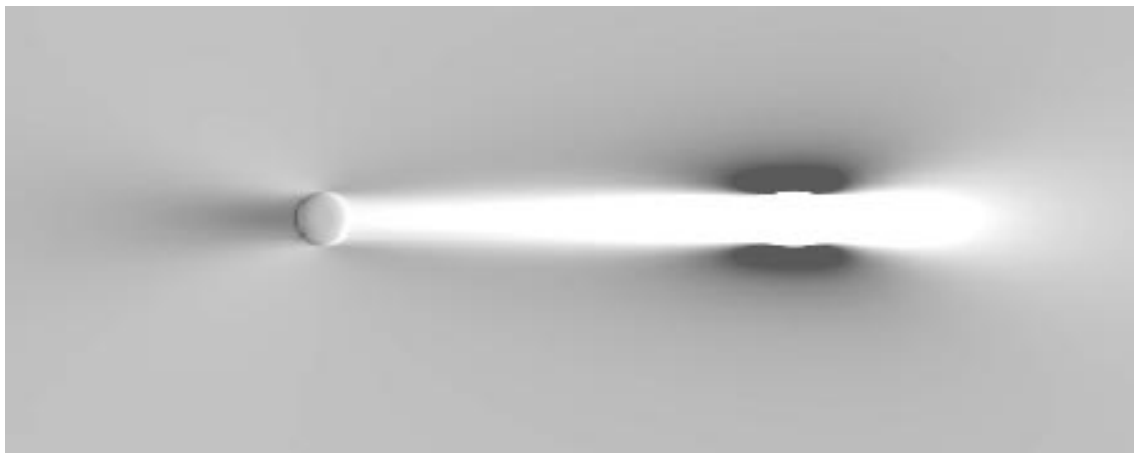


FIG. 3c

FIG. 3.—Example magnification maps show the ratio of planetary to single-lens magnification in the source plane. Light areas show positive deviations (ratios greater than 1), and dark areas show negative deviations. All panels are for  $q = 10^{-4}$ , a planet of 10 Earth masses around a  $0.3 M_{\odot}$  star. (a)  $x_p = 1.3$  with a source radius of  $u_* = 0.003$ ; (b)  $x_p < 1$  ( $x_p = 0.8$ ) with the same source radius; (c)  $x_p = 1.3$ , but with the large source radius of  $u_* = 0.03$ .

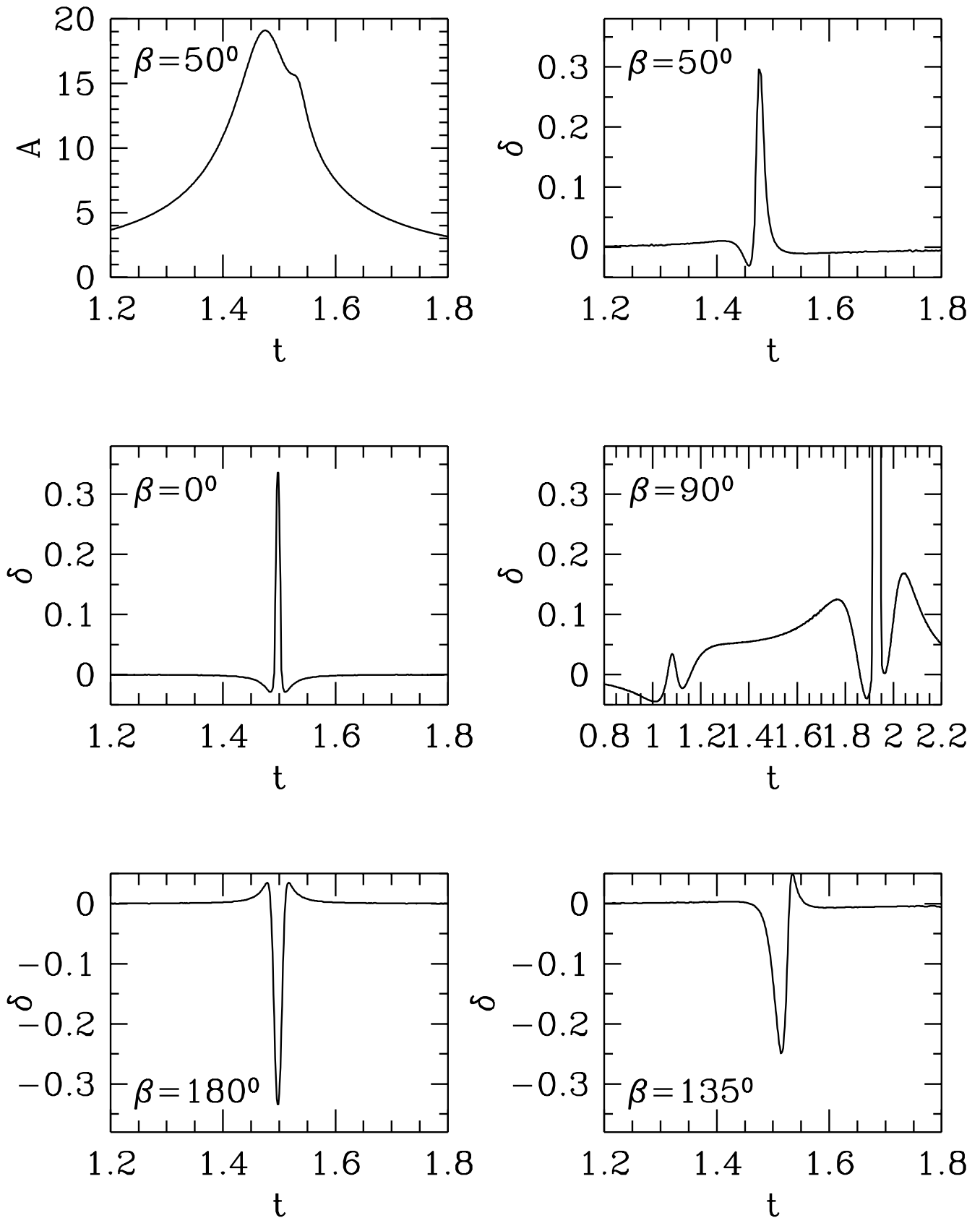


FIG. 4.—Example of high-magnification light curves, for  $q = 0.003$ ,  $x_p = 1.5$ ,  $u_{\min} = 0.05$ , and various angles of approach to the central caustic. The upper left-hand panel shows the total magnification light curve, while the others show only the deviation  $\delta = (A_{\text{binary}} - A_{\text{single}})/A_{\text{single}}$ . Time is plotted in units of  $t_E$ . The  $\beta = 0^\circ$  trajectory is perpendicular to the lens-planet axes and between them, while  $\beta = 180^\circ$  is on the side opposite the planet. As is apparent, the  $\beta = 90^\circ$  trajectory also hits the larger planetary caustic.

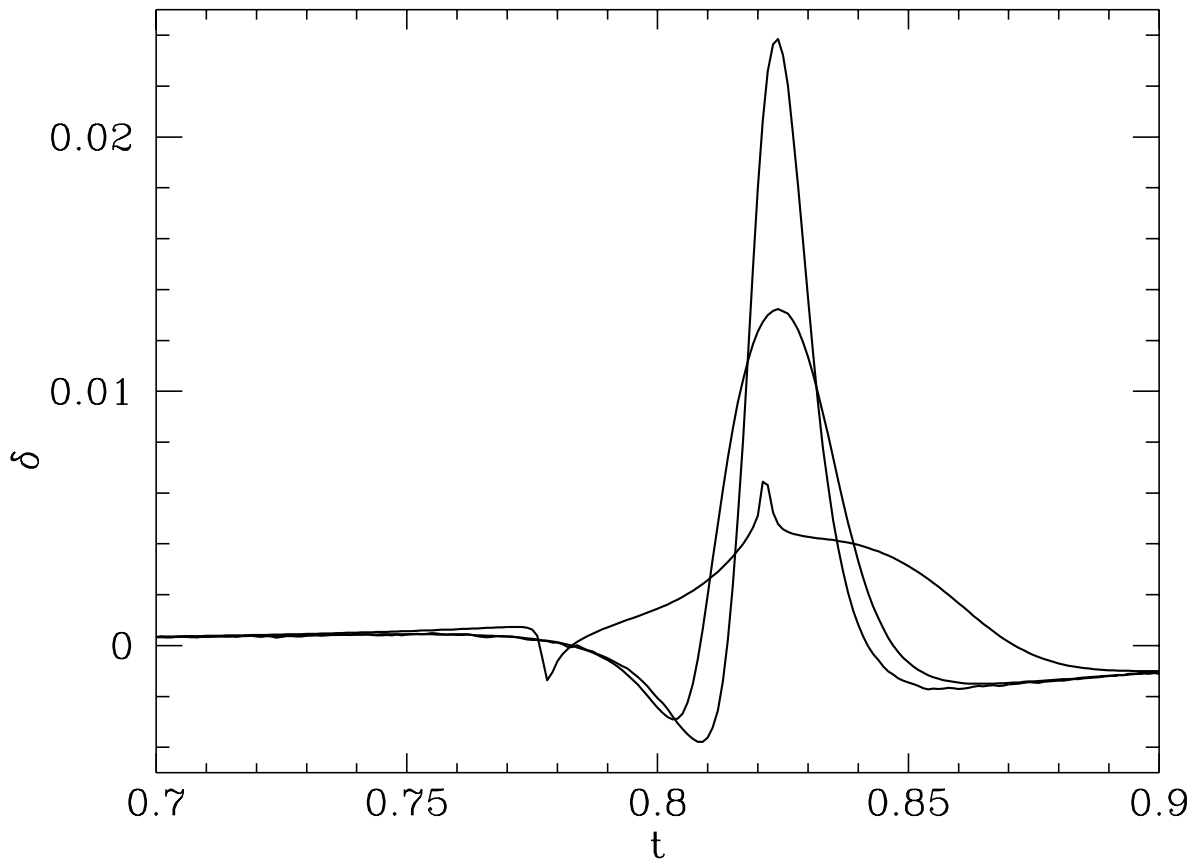


FIG. 5.—Comparison of planetary deviation light curve for different source radii:  $u_* = 0.003$ ,  $0.01$ , and  $0.03$ , corresponding to  $R_* = 3 R_\odot$  with lens at 4 kpc,  $R_* = 10 R_\odot$  with lens at 4 kpc, and  $R_* = 10 R_\odot$  with lens at 7 kpc, respectively. The deviation  $\delta$  is plotted vs. the time in units of  $t_E$ . These curves are for  $q = 10^{-4}$ ,  $x_p = 1.3$ ,  $u_{\min} = 0.02$ , and  $\beta = 50^\circ$ . The smaller the stellar radius, the higher and sharper the deviation. The bumps in the  $u_* = 0.03$  radius curve occur as the limb of the star crosses the central caustic.

allows the projected transverse velocity to be measured. For high-magnification events, the width (and height) of these bumps are determined by the size of the central caustic, and so information about  $q$  and  $x_p$  can also be gleaned. In Figures 3 and 5, however, the width of the ring and the bumps is determined not by the size of the central caustic but by the resolution of our underlying magnification map. Extraction of planetary parameters from high-magnification events will be discussed in more detail elsewhere (Griest & Safizadeh 1998).

### 3. DETECTING PLANETS

Current experiments to search for planets and other microlensing fine structure piggyback the very successful MACHO collaboration survey alert system (Alcock et al. 1996; Pratt et al. 1995). The MACHO collaboration monitors millions of stars each night and checks them for microlensing. When a candidate microlensing event is detected, an alert is sent by e-mail to any interested party.<sup>1</sup> Two main follow-up collaborations are underway: The MACHO GMAN collaboration (Alcock et al. 1996; Pratt et al. 1995) and the PLANET collaboration (Albrow et al. 1996). GMAN has detected parallax events, the finite source size, and proper motion fine structure, as well as several binary-lens events. PLANET has followed many events and detected much fine structure as well. Two new survey systems, EROS II and OGLE II, plan to soon generate

alerts, and new additions to the follow-up networks should make coverage of the short-duration planetary deviations more complete.

Several groups have now calculated the probabilities that a well-monitored microlensing alert will give rise to planetary fine structure. In calculating probabilities, workers calculated typical light curves caused by planetary systems and then defined a detection statistic. For example, Mao & Paczyński (1991) and Bolatto & Falco (1994) defined “detectable” as at least one light-curve point inside an area around the planetary caustic. Gould & Loeb (1992) considered a planet detectable if any point on the light curve deviated by more than 5% from the single-lens case. Bennett & Rhie (1996) defined detectable as the light curve deviating by more than 4% for a period of  $t_E/200$ . Gould & Loeb (1992) found that for a Jupiter-mass planet at a distance of 5 AU from its sun, the probability of detection thus defined was nearly 17%. Given that Jupiter’s mass is  $0.001 M_\odot$ , it was remarkable that the detection probability was so high. They explained this in terms of “resonant” lensing, which occurs when the planet is near the Einstein ring radius ( $x_p \approx 1$ ), and thus discovered the “lensing zone.” As discussed in detail in the Appendix, we define the lensing zone as the range  $0.618 \leq x_p \leq 1.618$ . For a Saturn-mass planet, their detection probability dropped to 3%, and for smaller mass planets, it was even smaller.

Although they performed a very complete calculation, Gould & Loeb made various approximations. For example, they did not calculate the deviation from a magnification

<sup>1</sup> <http://darkstar.astro.washington.edu>; [macho@astro.washington.edu](mailto:macho@astro.washington.edu).

map but approximated the region of 5% deviation as a long rectangular box in the source plane. They did not include finite source effects, which should not be large for the Jupiter-mass and Saturn-mass planets on which they concentrated, but which could be large for Uranus-mass or Earth-mass planets.

By including finite source size effects, Bennett & Rhie (1996) and Wambsganss (1997) continued the calculation to lower mass planets, where the finite size of the source star can be important. Bennett & Rhie found probabilities of about 2% for masses as low as Earth mass. Peale (1997), Tytler (1996), and Sackett (1997) calculated in detail the number of expected planetary detections for several realistic observing scenarios, and now several groups are undertaking extensive microlensing searches for planets. See Peale (1997), Sackett (1997), or Sahu (1997) for reviews. The basic plan is to monitor continuously all bulge stars undergoing microlensing with the hope of finding planetary signals in a few percent of them.

#### 4. HIGH-MAGNIFICATION EVENTS

Planetary magnification maps have their most pronounced deviations from single-lens maps near the planetary caustics. The size of these caustics scales directly with the planet-lens mass ratio, and they are located roughly at positions given by equation (A2). Thus, the probability of detecting a planet is roughly proportional to the angle-averaged cross-sectional area of this region, and this is how Mao & Paczyński (1991) and Bolatto & Falco (1994) calculated planetary detection probabilities. Gould & Loeb (1992) also pointed out that the region of large deviation continues on a line from the planetary caustic toward the primary lens.

Gould & Loeb state that in order to get a large deviation, the planet must come near one of the two primary-lens images. This is equivalent to saying that large deviations occur when the source is near the planetary caustics. In this paper, we point out that for high-magnification events, when the source comes very close to the very small central caustic, large deviations from a single-lens light curve also occur. Thus, even though the planet is not near one of the primary lens images, planet detection can occur. This is because the high magnification makes the small changes in the central caustic detectable. In summary, very close to the lens center, the difference between the circularly symmetric single-lens caustic and the tiny wedgelike binary central caustic causes measurable asymmetries in the light curve. Examples of these caustics are given in Figure 2, and example light curves are given in Figure 4. Note from Figure 4 that the structure of high-magnification light curves is typically simpler than the structure of planetary caustic crossing light curves.

In order to quantify this effect, we used our magnification maps to calculate a large number of light curves. For comparison purposes, we defined several “detection criteria.”  $P_5$  is the Gould & Loeb criterion that at least one point has a deviation of more than 5% from the single-lens case.  $P_4$  is our analog of the Bennett & Rhie criterion that the event have a time of at least  $t_E/200$  with more than a 4% deviation. As a challenge to observers, we also defined  $P_1$ , where the planet is assumed to be detectable if it spends a duration of at least  $t_E/200$  with a deviation from the single-lens case of at least 1%. The high magnification of the signal does make this criteria less demanding than for the more modest

magnification events usually considered. Finally, we define  $P_\chi$  using a  $\chi^2$  statistic. We define  $\chi_p^2 = \sum \delta_i^2$ , where the sum is over all points for which  $u < 0.2$ , that is, the total squared deviation for points during the time when  $A \geq 5$ . We define a planet as detectable if  $\chi_p^2 \geq 0.04$ , a number set by trial and error to correspond approximately to the sensitivity of  $P_5$  and  $P_4$ . If the photometric measurement errors were  $\sigma_i$ , this value would correspond to a  $\chi^2$  of  $0.04/\sigma_i^2$ .

Note that in calculating the deviation, Gould & Loeb subtracted a single lens at  $x_l = 0$  with the primary lens mass unchanged, while Bennett & Rhie subtracted a single lens of mass  $m_l + m_p$  at the center-of-mass position. We tried both of these subtraction schemes and did not find any significant difference. We use the deviation ratio  $\delta = (A_{\text{binary}} - A_{\text{single}})/A_{\text{single}}$ , since this quantity has constant magnitude errors as the magnification increases, close to what happens in a CCD observation.

To investigate high-amplification events, we took a sample of events with  $u_{\text{min}} \leq u_{\text{th}}$ , for  $u_{\text{th}} = 0.1, 0.05, 0.03,$  and  $0.02$ , corresponding, respectively, to single-lens magnifications of at least 10, 20, 33, and 50. The quantity  $u_{\text{min}}$  is the distance of closest approach of the source to the primary lens (in units of  $R_E$ ). The maximum magnification  $A_{\text{max}} \approx 1/u_{\text{min}}$  for  $A_{\text{max}} \gg 1$ . Given  $u_{\text{th}}$ , the probability of an event occurring with  $u_{\text{min}} \leq u_{\text{th}}$  is known a priori to be equal to  $u_{\text{th}}/u_{\text{crit}}$ , where it is assumed that every event with primary-lens magnification greater than  $A_{\text{crit}}$  is alerted on and monitored ( $u_{\text{crit}} = 1$  for  $A_{\text{crit}} = 1.34$ ). So, for example, with  $u_{\text{crit}} = 1$ , roughly 3% of monitored events will have  $u_{\text{min}} \leq 0.03$ . For each set of parameters, we created 18,000 light curves with angles of approach varying by  $1^\circ$  and 50 different values of  $u_{\text{min}}$ .

Figures 6, 7, 8, and 9 show the results of the probability calculations. Remarkable is the very high probability for detecting planets within the lensing zone. Figure 6 ( $q = 0.003$ ) shows a Jupiter-mass planet around a  $0.3 M_\odot$  star. Figure 7 ( $q = 0.001$ ) shows a Saturn-mass planet around a  $0.3 M_\odot$  star, or equivalently a Jupiter-mass planet around  $1 M_\odot$  star. Figure 8 ( $q = 10^{-4}$ ) shows a planet of 10 Earth masses around a  $0.3 M_\odot$  star.

For  $u_{\text{th}} = 0.02$  or  $0.03$ , and using  $P_5$ , the least sensitive of our detection criteria, basically 100% of Jupiter-mass planets would be detected over the entire lensing zone and substantially beyond it. As indicated by equation (3), the lensing-zone probabilities drop as  $u_{\text{th}}$  increases, and therefore  $A_{\text{max}}$  decreases to as low as 90% for  $u_{\text{th}} = 0.05$  and to as low as 80% for  $u_{\text{th}} = 0.1$ . The  $\chi_p^2$  statistic  $P_\chi$  performs similarly or slightly better than  $P_4$  and  $P_5$  over the entire range. If one could use  $P_1$  by detecting 1% deviations in the light curve, then the detection probabilities would remain near 100%, far beyond the lensing zone for all values of  $u_{\text{th}}$ .

For Saturn-mass planets, Figure 7 shows that probabilities are also near 100% inside the lensing zone, with a minimum of 90% for  $u_{\text{th}} = 0.02$  and a minimum of 80% detected for  $u_{\text{th}} = 0.03$ . The dropoff in sensitivity is quite rapid outside the lensing zone and for larger values of  $u_{\text{th}}$  but stays near 100% at  $x_p \approx 1$ , and above 40% even at the edge of the  $u_{\text{th}} = 0.1$  zone. If one could detect 1% deviations, then the probability is again nearly 100% over a wide range of  $x_p$ .

We note a duality invariance  $x_p \rightarrow 1/x_p$  in the probability plots for high-magnification events. The probability of detecting a planet at  $x_p = 0.5$  is the same as detecting a planet at  $x_p = 2$ . This is because the central caustic is almost

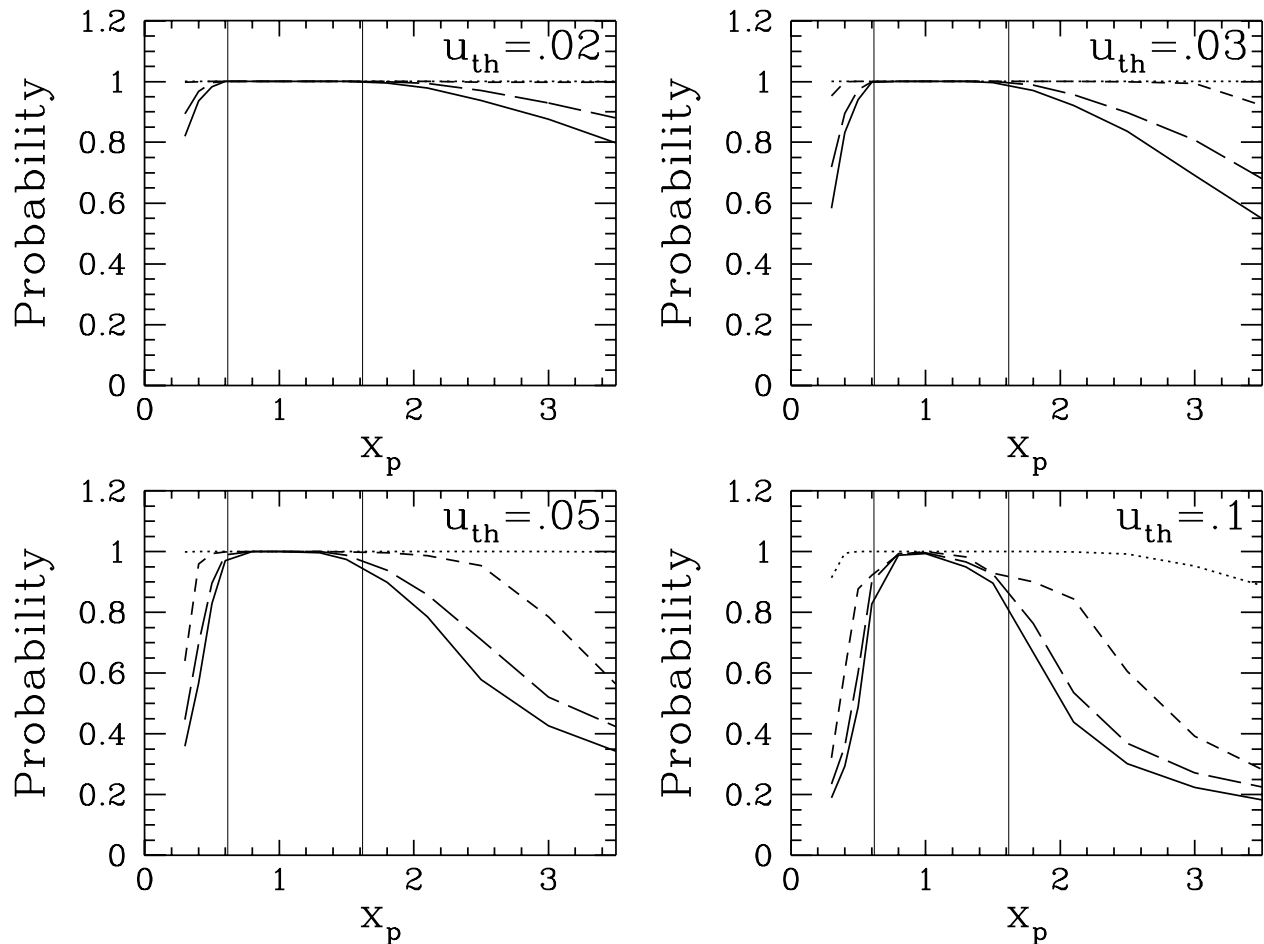


FIG. 6.—Probability of planetary detection for high-magnification events for a planet/lens mass ratio of  $q = 0.003$ , corresponding to a Jupiter-mass planet around a  $0.3 M_{\odot}$  star. The probability is plotted vs. the planet-lens separation  $x_p$  in units of  $R_E$ . Each panel shows a different value of threshold  $u_{th}$ , where only events that have  $u_{min} \leq u_{th}$  are counted. Four different detection statistics are plotted in each panel:  $P_5$  (solid line);  $P_4$  (long-dashed line);  $P_x$  (short-dashed line);  $P_1$  (dotted line). The light vertical lines demarcate the lensing zone.

identical under this transformation (see eq. [2] and Fig. 2). The duality symmetry also shows up in the position of the planetary caustics:  $x_p$  and  $1/x_p$  give caustics at the same  $x_c$  according to equation (A2) (see Fig. 1). This symmetry implies a degeneracy in determining the planet position from the light curve for high-magnification events. High-magnification light curves with a planet at  $x_p$  will be almost identical to those with a planet at  $1/x_p$  in most cases. There are also potential degeneracies between planetary mass and distance, and these will be considered elsewhere (Griest & Safizadeh 1998). See Gaudi & Gould (1997) for an extensive discussion of degeneracies for planetary caustic events.

Figures 8 and 9 show the probabilities for a planet of 10 Earth masses ( $q = 10^{-4} M_{\odot}$ ). From equation (2), we expect the size of the deviations to drop by a factor of 10 from the  $q = 0.001$  case, so we expect small probabilities when using  $P_4$  or  $P_5$ . Also, we expect statistics such as  $P_4$ , which require a minimum time above a threshold, to lose sensitivity in comparison with  $P_5$ , which requires only one deviant point. These expectations are borne out in Figure 8, which shows a maximum probability of  $\sim 80\%$  near  $x_p \approx 1$ , dropping rapidly even inside the lensing zone, and probabilities below 1% at the edge of the lensing zone.  $P_1$  fares much better, giving probabilities of 80%–100% near the zone center and dropping to 20%–50% near the zone edge.

In order to test the effect of the finite source size on our probabilities, we convolved each map with a kernel representing a limb-darkened source star of various radii and then recalculated the probabilities. For  $q = 0.003$ , we found no significant differences with radii up to  $u_* = 0.01$ , corresponding to a typical giant star at a distance halfway to the Galactic center. For  $q = 10^{-4}$ , however, the effect is quite apparent, as is shown in Figures 8 and 9. For  $u_* = 0.01$ , the peak  $P_5$  or  $P_4$  probabilities are less than 35% with a rapid drop even inside the lensing zone. In this case, the convolution has caused the maximum deviations due to the central caustic to drop below 4%, so that the detections are not actually “high-magnification” events but rather are caused by trajectories that pass through the planetary caustic region. This explains the counterintuitive result that the  $u_{th} = 0.1$  case has a higher probability than the  $u_{th} = 0.02$  case. Low values of  $u_{th}$  force the trajectories to pass near the origin, while higher values include trajectories that are more likely to hit the planetary caustic. If 1% deviations could be detected, the  $P_1$  statistic gives high probabilities even for planets of 10 Earth masses and giant source stars. The higher probabilities of Figure 8 show that the central caustic is still important for  $u_* = 0.003$ .

We note that all the probabilities calculated here are for the projected lens-planet separation. To find the probability

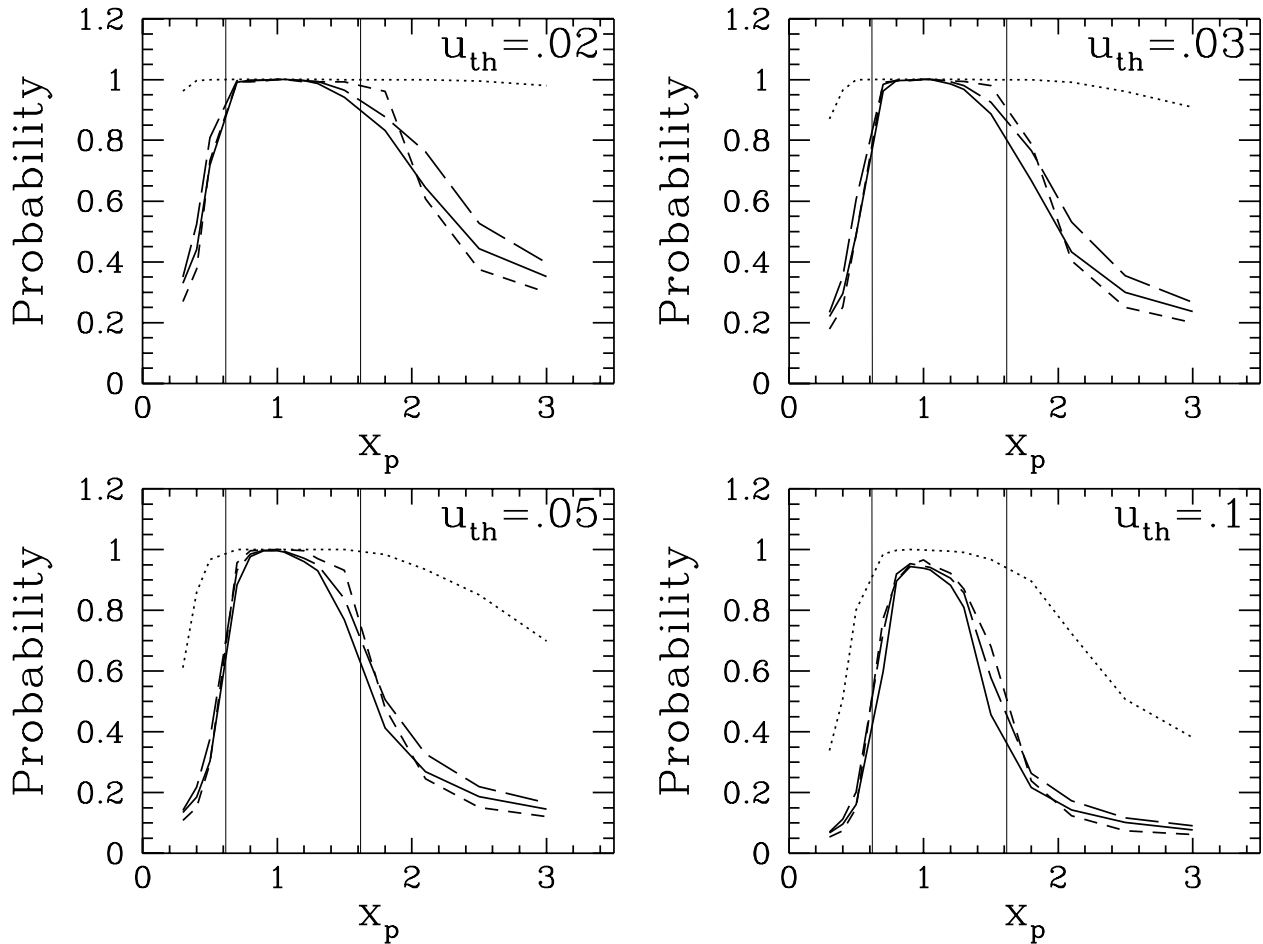


FIG. 7.—Same as Fig. 6, except for  $q = 0.001$ , corresponding to a Saturn-mass planet around a  $0.3 M_{\odot}$  star, or a Jupiter-mass planet around a  $1 M_{\odot}$  star

of detecting a planetary system with a given semimajor axis, our probabilities must be averaged over the possible inclination angles of the planetary system. To find the probability of finding a planet of a given mass, one must then average over a distribution of semimajor axes and also over the density of planetary systems along the line of sight, taking into account the variation of  $x'$ . See Gould & Loeb (1992) for an example. This calculation will be presented elsewhere (Griest & Safizadeh 1998), but see § 6 for a caveat.

## 5. DISCUSSION

High-magnification events have both advantages and disadvantages when compared with ordinary planetary fine-structure events. One obvious advantage is that since the source star is highly magnified, more flux is available and more accurate photometry can be performed. For example, events satisfying the  $u_{\text{th}} = 0.03$  or  $u_{\text{th}} = 0.02$  criteria are 3–4 mag brighter during peak magnification, and thus Poisson errors in the photometry are reduced. The obvious disadvantage is that high-magnification events occur rarely, only 2%–3% of the time for the above examples, so the number of such events will be small. In some situations, this disadvantage may be somewhat offset since fewer telescope resources will be needed to perform the follow-up. Typical groups searching for planets anticipate monitoring dozens of events per day in a round-the-clock manner since it is never known when a few-hour-long planetary excursion

will take place. This requires a worldwide system of dedicated telescopes. Since the time of a high-magnification peak can be predicted well in advance, a focus on high-magnification events would allow concentration of resources on the most valuable events.

Larger telescopes that allowed rapid rescheduling could more easily be brought into play if the time needed was small and the potential payoff large. It might be worth deploying special-purpose equipment to reach more sensitive detection thresholds if the chances of success were known to be large.

So, while continuous monitoring is crucial for giving the maximum total detections, special attention should be given to high-magnification events since the cost/benefit ratio is better. In addition, the high probability of detection results in a high-efficiency experiment and allows nearly definitive statements to be made on a system-by-system basis. For example, using Figure 6, each nondetection in an  $A_{\text{max}} > 33$  event immediately implies that there is no planet with a mass equal to or greater than Jupiter in the lensing zone. The high efficiency also allows statistical results to be obtained with fewer actual measurements. Another potential advantage of high-magnification events is the larger likelihood of a measurable finite source size effect. In these cases, the projected transverse proper motion can be found, and information about the lens distance ( $x'$ ) can be inferred. This can help break the degeneracies, described in Gaudi & Gould (1997), that make determination of  $q$  and  $x_p$  difficult.

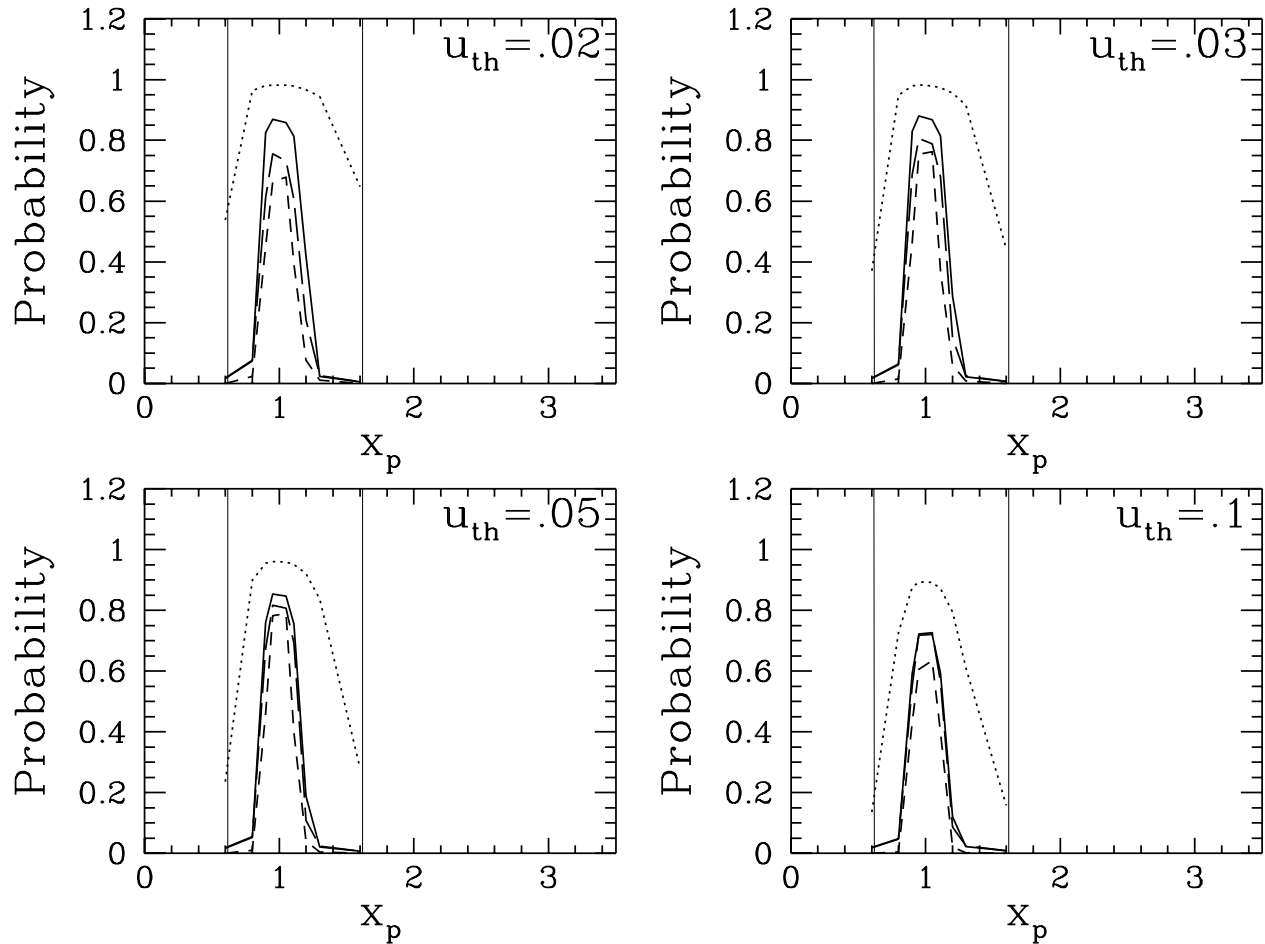


FIG. 8.—Same as Fig. 6, except for  $q = 10^{-4}$ , corresponding to a planet of 10 Earth masses or a Uranus-mass planet around a  $0.3 M_{\odot}$  star. The source is  $u_* = 0.003$ .

#### 6. LIGHT-CURVE FITTING VERSUS A PRIORI SUBTRACTION

All probability predictions made to date have used the deviation between the binary-lens light curve and the single-lens light curve as the signal to be detected. In this paper, we followed suit so as to allow comparison of our probabilities with previous calculations. In practice, however, only the observed binary light curve (plus noise) is known. In order to extract the signal, one can subtract a single-lens light curve, but one does not know a priori which single-lens light curve to subtract. It must be found by fitting, and the fitted single-lens light curve will try to minimize the binary features and will reduce the signal. In order to test the size of this effect, we performed a nonlinear fit to a single-lens light curve and then subtracted that light curve. Examples of the residuals from such subtractions are shown in Figure 10. The effect described above is clear. The  $\chi^2$  fitting procedure produces a single-lens light curve that minimizes the largest deviations; in  $\chi^2$  fitting it is better to miss many points by a little than a few points by a lot. When using threshold detection criteria, as was done here and as has

been done by previous workers, the detection probability can be altered. In the example of Figure 10, the peak deviation is above the  $P_5$  detection threshold of 0.05 when using a priori subtraction but below even the  $P_4$  threshold of 0.04 when using the fit subtraction. Thus, we counted this event as detectable in our calculations, while it would not be detectable by these criteria if the fit subtraction was used. This effect holds not only for high-magnification events but for all planet detection probabilities near the detection threshold. There may be other detection statistics that are more robust to fitting, and these will be explored elsewhere (Griest & Safizadeh 1998).

K. G. thanks Jerry Guern for many helpful conversations and work on early versions of these calculations. We thank Neal Dalal for help on the size of the central caustics, the use of his caustic-finding program, and other useful conversations. We thank Art Wolfe for the use of his computer. We acknowledge support from an IGPP minigrant, from the Department of Energy, from the Alfred P. Sloan Foundation, and from a Cottrell Scholar award of the Research Corporation.

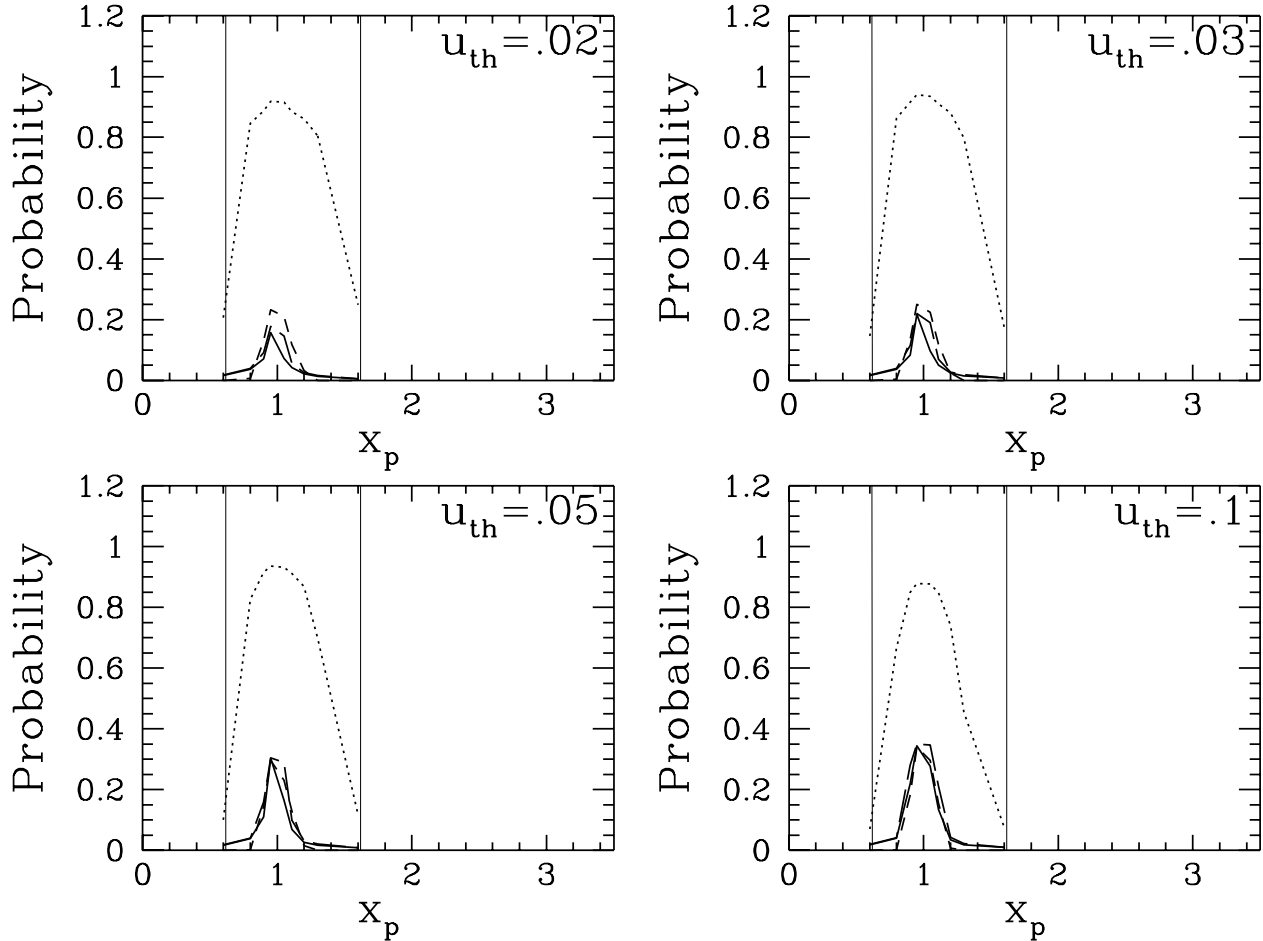


FIG. 9.—Same as Fig. 8, except that the source radius is  $u_* = 0.01$ , corresponding to a giant source star

## APPENDIX A

### PLANETARY CAUSTIC POSITIONS, THE LENSING ZONE, AND CENTRAL CAUSTIC SIZE

Consider a single pointlike lens at  $x = 0$  and a source at  $x_s$ . The two images occur along the lens-source line at

$$x_i = [x_s \pm (x_s^2 + 4)^{1/2}]/2, \quad (\text{A1})$$

where all distances are measured in units of  $R_E$ . A negative value of  $x_i$  means the image is on the other side of the lens from the source.

Since a planet mass is much smaller than the primary-lens mass, its area of influence is small when measured in units of  $R_E$ . Thus, to first approximation the planet can have a large effect only when its position is near one of the main images ( $x_i$ ). This is the lens plane point of view. From the source plane point of view, one expects the planet to have a strong effect when the source comes near the planetary caustics (for example, see Fig. 1). Thus, the strong effect of the source being near the planetary caustic is the same as the planet being near one of the single-lens images. The relation between planet and caustic positions should then be the same as the relation between image and source positions, that is, the inverse of equation (A1). Thus the caustic position is along the  $x$ -axis at

$$x_c \simeq (x_p^2 - 1)/x_p, \quad (\text{A2})$$

where  $x_p$  is the position of the planet in units of  $R_E$ . This formula should work when  $m_p \ll m_l$  and  $x_p$  is not near unity. When  $m_l \approx m_p$ , the planetary influence is no longer small, and when  $x_p \approx 1$ , the caustics merge and take complicated shapes.

The “lensing zone” was first discussed by Gould & Loeb (1992) as the set of planet-lens distances where the probability of detecting the planet was high (see their Fig. 4), and it has been used with various definitions by others to mean the region where the planet is near the Einstein ring. In searching for planets, one requires as a selection criterion that the primary lens be magnified by more than some amount such as  $A_{\text{th}} = 1.34$ . This is because, observationally, microlensing is not easy to identify when the peak magnification is low. This selection criterion is equivalent to requiring that the source star pass within some (projected) distance of the primary lens (e.g.,  $u_{\text{th}} = 1$ , for  $A_{\text{th}} = 1.34$ ). The probability of detecting the planet is proportional to the averaged cross section of some magnification contour in the source plane, which is roughly proportional to the chance that a trajectory that comes within  $u_{\text{th}}$  also hits the planetary caustic. When the caustic is near the Einstein ring ( $x_c \approx 1$ ), the probability is high, and when the caustic is within the ring ( $x_c < 1$ ), the probability is also high, but when the caustic is far

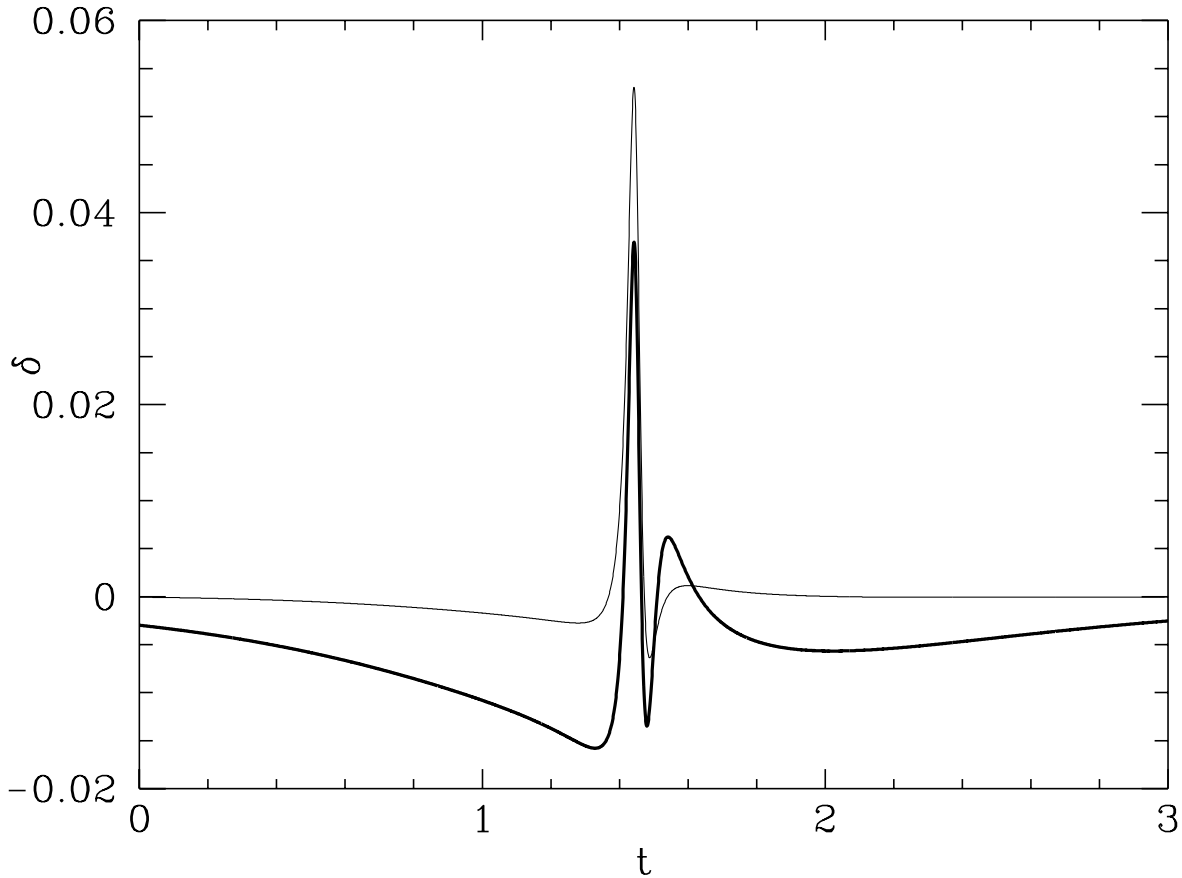


FIG. 10.—Comparison of planetary deviation light curve when using fitting to find the single-lens subtraction light curve and when using the known single-lens light curve. The quantity  $\delta = (A_{\text{binary}} - A_{\text{single}})/A_{\text{single}}$  is plotted vs. the time in units of  $t_E$ . The light line uses the known single-lens parameters in the  $\delta$ -subtraction, while the heavy line finds the best-fit single-lens parameters from the binary light curve. The fit light curve is less likely to be detected when threshold statistics are used. Parameters are  $q = 0.001$ ,  $x_p = 1.5$ ,  $u_{\text{min}} = 0.05$ , and  $\beta = 50^\circ$ .

outside the ring ( $x_c \gg 1$ ), the probability drops at least inversely with distance  $x_c$ . Thus, the lensing zone can be defined as those positions  $x_p$  for which  $x_c \leq 1$ . Using equation (A2), this definition corresponds to a lensing zone of  $0.618 < |x_p| < 1.618$ , values also used by Wambsganss (1997). While the detection probability drops quickly outside the lensing zone, clearly there will be some probability when the caustic is just outside the Einstein ring. Also, the probability near the edge of the zone will be smaller than in the middle. Finally, since the mass of the planet determines the caustic size and region of influence, the edges of the zone will be a strong function of the mass of the planet and also of the detection criteria used.

The extent of the central caustic along the  $x$ -axis (Fig. 2) can be estimated as follows. For a single pointlike lens, the image of the pointlike caustic is the circular Einstein ring critical curve of radius 1. When  $q = m_p/m_l \ll 1$  and  $x_p \neq 1$ , we expect the binary system critical curve to remain nearly the same and to map onto the small central caustic (see Fig. 2). The planetary caustics will map onto one or two small critical curves near the planet.

Restricting ourselves to the  $x$ -axis, the planet will affect the central caustic in two ways. First, the critical curve that crosses the  $x$ -axis at  $x = \pm 1$  in the single-lens case will be moved slightly to  $x = \pm 1 + \epsilon$ . Second, the planet will cause the critical curve image to map to a slightly different position on the  $x$ -axis. Equation (5) says the tip of the central caustic on the  $x$ -axis will occur at  $x_s = x - 1/x + q/(x_p - x)$ . To find  $x$ , we find the critical curve using equation (6) and  $A_i = \infty$ , or

$$1 - \left[ \frac{1}{x^2} + \frac{q}{(x - x_p)^2} \right]^2 = 0. \quad (\text{A3})$$

Let  $x = 1 + \epsilon$ , and solve this equation in the limit of  $q \ll 1$  ( $m_p \ll m_l$ ) and  $\epsilon \ll 1$  (the critical curve does not move much). This gives

$$\epsilon \simeq \frac{q}{2(1 - x_p)^2} \left[ 1 + \frac{q}{(1 - x_p)^3} \right]^{-1} \simeq \frac{q}{2(1 - x_p)^2}. \quad (\text{A4})$$

Inserting  $x = 1 + \epsilon$  into equation (5) gives

$$u_c \equiv x_s \simeq 2\epsilon + \frac{q}{x_p - 1} \simeq \frac{qx_p}{(x_p - 1)^2}. \quad (\text{A5})$$

This is the expected shift from the origin for the caustic tip. This formula gives a very good prediction of the sizes of the caustics shown in Figure 2. Note that the formula is invariant under the transformation  $x_p \rightarrow 1/x_p$  as evidenced in Figure 2, and displayed in equation (2). We expect the formula to break down when  $q \rightarrow 1$  or  $x_p \rightarrow 1$ .

## REFERENCES

- Alard, C., et al. 1995, *A&A*, 300, L17  
 Albrow, M., et al. 1996, preprint (astro-ph/9610128)  
 Alcock, C., et al. 1993, *Nature*, 365, 621  
 ———. 1995, *ApJ*, 454, L125  
 ———. 1996, *ApJ*, 463, L67  
 ———. 1997a, *ApJ*, 479, 119  
 ———. 1997b, *ApJ*, 490, L59  
 Aubourg, E., et al. 1993, *Nature*, 365, 623  
 Bennett, D. P., & Rhie, S. H. 1996, *ApJ*, 472, 660  
 Bolatto, D. B., & Falco, E. E. 1994, *ApJ*, 436, 112  
 Gaudi, B. S., & Gould, A. 1997, *ApJ*, 486, 85  
 Gould, A. 1992, *ApJ*, 392, 442  
 ———. 1994a, *ApJ*, 421, L71  
 ———. 1994b, *ApJ*, 421, L75  
 Gould, A., & Gauchere, C. 1997, *ApJ*, 477, 580  
 Gould, A., & Loeb, A. 1992, *ApJ*, 396, 104  
 Griest, K. 1991, *ApJ*, 366, 412  
 Griest, K., & Safizadeh, N. 1998, in preparation  
 Mao, S., & Paczyński, B. 1991, *ApJ*, 374, L37  
 Nemiroff, R. J., & Wickramasinghe, W. A. D. T. 1994, *ApJ*, 424, L21  
 Paczyński, B. 1986, *ApJ*, 304, 1  
 Peale, S. J. 1997, *Icarus*, 127, 269  
 Pratt, M. R., et al. 1995, in *IAU Symp. 173, Astrophysical Applications of Gravitational Lensing*, ed. C. S. Kochanek & J. N. Hewitt (Dordrecht: Kluwer)  
 Sackett, P. D. 1997, preprint (astro-ph/9709269)  
 Sahu, K.C. 1997, preprint (astro-ph/9704168)  
 Tytler, D. 1996, in *Road Map for Exploration of Neighboring Planetary Systems* (Jet Propulsion Lab. publ. preprint 92-22)  
 Udalski, A., et al. 1993, *Acta Astron.*, 43, 289  
 ———. 1994, *ApJ*, 436, L103  
 Wambsganss, J. 1997, *MNRAS*, 284, 172  
 Witt, H. J. 1990, *A&A*, 236, 311  
 Witt, H. J., & Mao, S. 1994, *ApJ*, 430, 505